

Efficient Subclass Segmentation in Medical Images

Linrui Dai¹, Wenhui Lei^{1,2}, and Xiaofan Zhang^{1,2,*}

¹Shanghai Jiao Tong University

²Shanghai Artificial Intelligence Laboratory
{o.o111, wenhui.lei, xiaofan.zhang}@sjtu.edu.cn

Abstract. As research interests in medical image analysis become increasingly fine-grained, the cost for extensive annotation also rises. One feasible way to reduce the cost is to annotate with coarse-grained superclass labels while using limited fine-grained annotations as a complement. In this way, fine-grained data learning is assisted by ample coarse annotations. Recent studies in classification tasks have adopted this method to achieve satisfactory results. However, there is a lack of research on efficient learning of fine-grained subclasses in semantic segmentation tasks. In this paper, we propose a novel approach that leverages the hierarchical structure of categories to design network architecture. Meanwhile, a task-driven data generation method is presented to make it easier for the network to recognize different subclass categories. Specifically, we introduce a Prior Concatenation module that enhances confidence in subclass segmentation by concatenating predicted logits from the superclass classifier, a Separate Normalization module that stretches the intra-class distance within the same superclass to facilitate subclass segmentation, and a HierarchicalMix model that generates high-quality pseudo labels for unlabeled samples by fusing only similar superclass regions from labeled and unlabeled images. Our experiments on the BraTS2021 and ACDC datasets demonstrate that our approach achieves comparable accuracy to a model trained with full subclass annotations, with limited subclass annotations and sufficient superclass annotations. Our approach offers a promising solution for efficient fine-grained subclass segmentation in medical images. Our code is publicly available [here](#).

Keywords: Automatic Segmentation · Deep Learning.

1 Introduction

In recent years, the use of deep learning for automatic medical image segmentation has led to many successful results based on large amounts of annotated training data. However, the trend towards segmenting medical images into finer-grained classes (denoted as *subclasses*) using deep neural networks has resulted in an increased demand for finely annotated training data [4, 11, 21]. This process requires a higher level of domain expertise, making it both time-consuming

*Corresponding author.

and demanding. As annotating coarse-grained (denoted as *superclasses*) classes is generally easier than subclasses, one way to reduce the annotation cost is to collect a large number of superclasses annotations and then labeling only a small number of samples in subclasses. Moreover, in some cases, a dataset may have already been annotated with superclass labels, but the research focus has shifted towards finer-grained categories [9, 24]. In such cases, re-annotating an entire dataset may not be as cost-effective as annotating only a small amount of data with subclass labels.

Here, the primary challenge is to effectively leverage superclass annotations to facilitate the learning of fine-grained subclasses. To solve this problem, several works have proposed approaches for recognizing new subclasses with limited subclass annotations while utilizing the abundant superclass annotations in classification tasks [6, 8, 18, 25]. In general, they assume the subclasses are not known during the training stage and typically involve pre-training a base model on superclasses to automatically group samples of the same superclass into several clusters while adapting them to finer subclasses during test time.

However, to the best of our knowledge, there has been no work specifically exploring learning subclasses with limited subclass and full superclass annotations in semantic segmentation task. Previous label-efficient learning methods, such as semi-supervised learning [7, 17, 26], few-shot learning [10, 15, 19] and weakly supervised learning [13, 27], focus on either utilize unlabeled data or enhance the model’s generalization ability or use weaker annotations for training. However, they do not take into account the existence of superclasses annotations, making them less competitive in our setting.

In this study, we focus on the problem of efficient subclass segmentation in medical images, whose goal is to segment subclasses under the supervision of limited subclass and sufficient superclass annotations. Unlike previous works such as [6, 8, 18, 25], we assume that the target subclasses and their corresponding limited annotations are available during the training process, which is more in line with practical medical scenarios.

Our main approach is to utilize the hierarchical structure of categories to design network architectures and data generation methods that make it easier for the network to distinguish between subclass categories. Specifically, we propose 1) a **Prior Concatenation** module that concatenates predicted logits from the superclass classifier to the input feature map before subclass segmentation, serving as prior knowledge to enable the network to focus on recognizing subclass categories within the current predicted superclass; 2) a **Separate Normalization** module that aims to stretch the intra-class distance within the same superclass, facilitating subclass segmentation; 3) a **HierarchicalMix** module inspired by GuidedMix [23], which for the first time suggests fusing similar labeled and unlabeled image pairs to generate high-quality pseudo labels for the unlabeled samples. However, GuidedMix selects image pairs based on their similarity and fuses entire images. In contrast, our approach is more targeted. We mix a certain superclass region from an image with subclass annotation to the corresponding superclass region in an unlabeled image without subclass annotation,

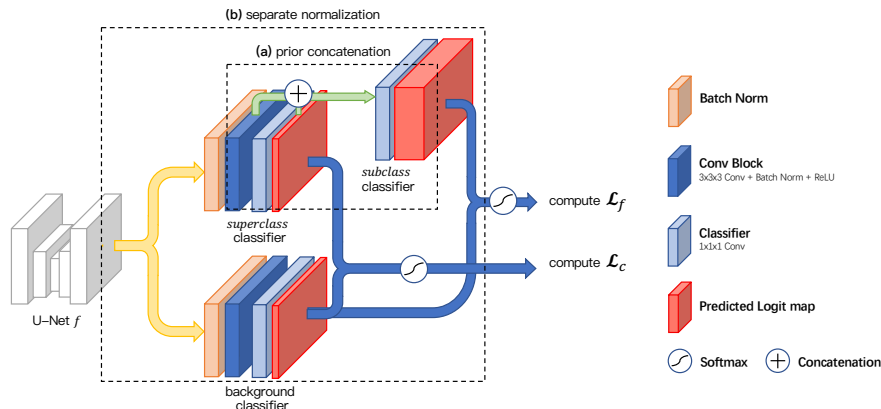


Fig. 1: Proposed network architecture, \mathcal{L}_c and \mathcal{L}_f stand for the superclass loss and subclass loss respectively.

avoiding confusion between different superclass regions. This allows the model to focus on distinguishing subclasses within the same superclass. Our experiments on the Brats 2021 [3] and ACDC [5] datasets demonstrate that our model, with sufficient superclass and very limited subclass annotations, achieves comparable accuracy to a model trained with full subclass annotations.

2 Method

Problem Definition We start by considering a set of R coarse classes, denoted by $\mathcal{Y}_c = \{Y_1, \dots, Y_R\}$, such as background and brain tumor, and a set of N training images, annotated with \mathcal{Y}_c , denoted by $\mathcal{D}_c = \{(x^l, y^l) | y_i^l \in \mathcal{Y}_c\}_{i=1}^N$. Each pixel i in image x^l is assigned a superclass label y_i^l . To learn a finer segmentation model, we introduce a set of fine subclass $K = \sum_{i=1}^R k_i$ in coarse classes, denoted by $\mathcal{Y}_f = \{Y_{1,1}, \dots, Y_{1,k_1}, \dots, Y_{R,1}, \dots, Y_{R,k_R}\}$, such as background, enhancing tumor, tumor core, and whole tumor. We assume that only a small subset of n training images have pixel-wise subclass labels $z \in \mathcal{Y}_f$ denoted by $\mathcal{D}_f = \{(x^l, z^l) | z_i^l \in \mathcal{Y}_f\}_{i=1}^n$. Our goal is to train a segmentation network $f(x^l)$ that can accurately predict the subclass labels for each pixel in the image x^l , even when $n \ll N$. **Without specification, we consider $R = 2$ (background and foreground) and extend the foreground class to multi subclass in this work.**

Prior Concatenation One direct way to leverage the superclass and subclass annotations simultaneously is using two $1 \times 1 \times 1$ convolution layers as superclass and subclass classification heads for the features extracted from the network. The superclassification and subclassification heads are individually trained by superclass $P_c(x^l)$ labels and subclass labels $P_f(x^l)$. With enough superclass labels, the

feature maps corresponding to different superclasses should be well separated. However, this coerces the subclassification head to discriminate among K subclasses under the mere guidance from few subclass annotations, making it prone to overfitting.

Another common method to incorporate the information from superclass annotations into the subclassification head is negative learning [14]. This technique penalizes the prediction of pixels being in the wrong superclass label, effectively using the superclass labels as a guiding principle for the subclassification head. However, in our experiments, we found that this method may lead to lower overall performance, possibly due to unstable training gradients resulting from the uncertainty of the subclass labels.

To make use of superclass labels without affecting the training of the subclass classification head, we propose a simple yet effective method called **Prior Concatenation (PC)**: as shown in Fig. 1 (a), we concatenate predicted superclass logit scores $S_c(x^l)$ onto the feature maps $F(x^l)$ and then perform subclass segmentation. The intuition behind this operation is that by concatenating the predicted superclass probabilities with feature maps, the network is able to leverage the prior knowledge of the superclass distribution and focus more on learning the fine-grained features for better discrimination among subclasses.

Separate Normalization Intuitively, given sufficient superclass labels in supervised learning, the superclassification head tends to reduce feature distance among samples within the same superclass, which conflicts with the goal of increasing the distance between subclasses within the same superclass. To alleviate this issue, we aim to enhance the internal diversity of the distribution within the same superclass while preserving the discriminative features among superclasses.

To achieve this, we propose **Separate Normalization(SN)** to separately process feature maps belonging to hierarchical foreground and background divided by superclass labels. As a superclass and the subclasses within share the same background, the original conflict between classifiers is transferred to finding the optimal transformations that separate foreground from background, enabling the network to extract class-specific features while keeping the features inside different superclasses well-separated.

Our framework is shown in Fig. 1 (b). First, we use Batch Norm layers [12] to perform separate affine transformations on the original feature map. The transformed feature maps, each representing a semantic foreground and background, are then passed through a convolution block for feature extraction before further classification. The classification process is coherent with the semantic meaning of each branch. Namely, the foreground branch includes a superclassifier and a subclassifier that classifies the superclass and subclass foreground, while the background branch is dedicated solely to classify background pixels. Finally, two separate network branches are jointly supervised by segmentation loss on super- and subclass labels. The aforementioned prior concatenation continues to take effect by concatenating predicted superclass logits on the inputs of subclassifier.

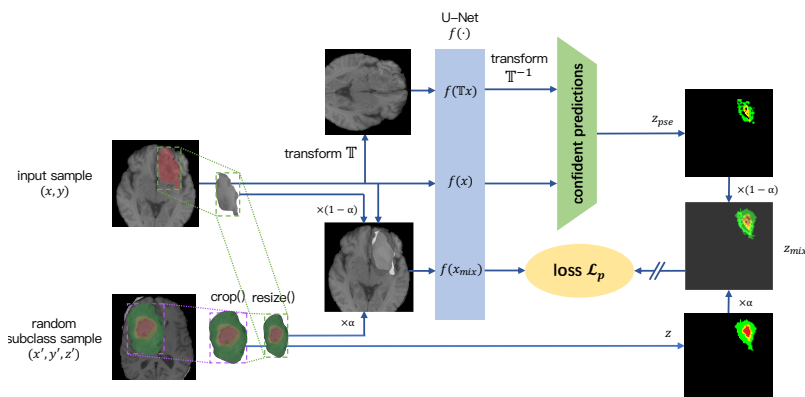


Fig. 2: The framework of *HierarchicalMix*. This process is adopted at training time to pair each coarsely labeled image x with its mixed image x_{mix} and pseudo subclass label z . “//” represents the cut of gradient backpropagation.

HierarchicalMix Given the scarcity of subclass labels, we intend to maximally exploit the existent subclass supervision to guide the segmentation of coarsely labeled samples. Inspired by GuidedMix [23], which provides consistent knowledge transfer between similar labeled and unlabeled images with pseudo labeling, we propose **HierarchicalMix(HM)** to generate robust pseudo supervision. Nevertheless, GuidedMix relies on image distance to select similar images and performs a whole-image mixup, which loses focus on the semantic meaning of each region within an image. We address this limitation by exploiting the additional superclass information for a more targeted mixup. This information allows us to fuse only the semantic foreground regions, realizing a more precise transfer of foreground knowledge. A detailed pipeline of HierarchicalMix is described below.

As shown in Fig. 2, for each sample (x, y) in the dataset that does not have subclass labels, we pair it with a randomly chosen fine-labeled sample (x', y', z') . First, we perform a random rotation and flipping \mathbb{T} on (x, y) and feed both the original sample and the transformed sample $\mathbb{T}x$ into the segmentation network f . An indirect segmentation of x is obtained by performing the inverse transformation \mathbb{T}^{-1} on the segmentation result of $\mathbb{T}x$. A transform-invariant pseudo subclass label map z_{pse} is generated according to the following scheme: Pixel (i, j) in z_{pse} is assigned a valid subclass label index $(z_{pse})_{i,j} = f(x)_{i,j}$ only when $f(x)_{i,j}$ agrees with $[\mathbb{T}^{-1}f(\mathbb{T}x)]_{i,j}$ with a high confidence τ as well as $f(x)_{i,j}$ and $x_{i,j}$ both belong to the same superclass label.

Next, we adopt image mixup by cropping the bounding box of foreground pixels in x' , resizing it to match the size of foreground in x , and linearly overlaying them by a factor of α on x . This semantically mixed image x_{mix} has subclass labels $z = \text{resize}(\alpha \cdot z')$ from the fine-labeled image x' . Then, we pass it through the network to obtain a segmentation result $f(x_{mix})$. This segmentation result

is supervised by the superposition of the pseudo label map z_{pse} and subclass labels z , with weighting factor α : $\mathcal{L}_p = \mathcal{L}(f(x_{mix}), \alpha \cdot z + (1 - \alpha) \cdot z_{pse})$.

The intuition behind this framework is to simultaneously leverage the information from both unlabeled and labeled data by incorporating a more robust supervision from transform-invariant pseudo labels. While mixing up only the semantic foreground provides a way of exchanging knowledge between similar foreground objects while lifting the confirmation bias in pseudo labeling [1].

3 Experiments

Dataset and preprocessing We conduct all experiments on two public datasets. The first one is the **ACDC*** dataset [5], which contains 200 MRI images with segmentation labels for left ventricle cavity (LV), right ventricle cavity (RV), and myocardium (MYO). Due to the large inter-slice spacing, we use 2D segmentation as in [2]. We adopt the processed data and the same data division in [16], which uses 140 scans for training, 20 scans for validation and 40 scans for evaluation. During inference, predictions are made on each individual slice and then assembled into a 3D volume. The second is the **BraTS2021[†]** dataset [3], which consists of 1251 mpMRI scans with an isotropic 1 mm³ resolution. Each scan includes four modalities (FLAIR, T1, T1ce, and T2), and is annotated for necrotic tumor core (TC), peritumoral edematous/invaded tissue (PE), and the GD-enhancing tumor (ET). We randomly split the dataset into 876, 125, and 250 cases for training, validation, and testing, respectively. For both datasets, image intensities are normalized to values in [0, 1] and the foreground superclass is defined as the union of all foreground subclasses for both datasets.

Implementation details and evaluation metrics To augment the data during training, we randomly cropped the images with a patch size of 256×256 for the ACDC dataset and $96 \times 96 \times 96$ for the BraTS2021 dataset. The model loss \mathcal{L} is set by adding the losses from Cross Entropy Loss and Dice Loss.

We trained the model for 40,000 iterations using SGD optimizer with a 0.9 momentum and a linearly decreasing learning rate that starts at 0.01 and ends with 0. We used a batch size of 24 for the ACDC dataset and 4 for the BraTS2021 dataset, where half of the samples are labeled with subclasses and the other half only labeled with superclasses. More details can be found in the supplementary materials. To evaluate the segmentation performance, we used two widely-used metrics: the Dice coefficient (DSC) and 95% Hausdorff Distance (HD_{95}). The confidence factor τ mentioned in HierarchicalMix starts at 1 and linearly decays to 0.4 throughout the training process, along with a weighting factor α sampled according to the uniform distribution on [0.5, 1].

*<https://www.creatis.insa-lyon.fr/Challenge/acdc/databases.html>

[†]<http://braintumorsegmentation.org/>

Performance comparison with other methods To evaluate the effectiveness of our proposed method, we firstly trained two **U-Net** models [20] to serve as upper and lower bounds of performance. The first U-Net was trained on the complete subclass dataset $\{(x^l, y^l, z^l)\}_{l=1}^N$, while the second was trained on its subset $\{(x^l, y^l, z^l)\}_{l=1}^n$. Then, we compared our method with the following four methods, all of which were trained using n subclass labels and N superclass labels: **Modified U-Net (Mod)**: This method adds an additional superclass classifier alongside the subclass classifier in the U-Net. **Negative Learning (NL)**: This method incorporates superclass information into the loss module by introducing a separate negative learning loss in the original U-Net. This additional loss penalizes pixels that are not segmented as the correct superclass. **Cross Pseudo Supervision (CPS)** [7]: This method simulates pseudo supervision by utilizing the segmentation results from two models with different parameter initializations, and adapts their original network to the Modified U-Net architecture. **Uncertainty Aware Mean Teacher (UAMT)** [26]: This method modifies the classical mean teacher architecture [22] by adapting the teacher model to learn from only reliable targets while ignoring the rest, and also adapts the original network to the Modified U-Net architecture.

Table 1: Mean Dice Score (% , left) and HD_{95} (mm, right) of different methods on ACDC and BraTS2021 datasets. Sup. and Sub. separately represents the number of data with superclass and subclass annotations in the experiments. ‘_’ means the result of our proposal is significantly better than the closet competitive result (p-value < 0.05). The standard deviations of each metric are recorded in the supplementary materials.

Method	ACDC								BraTS2021					
	Sup.	Sub.	RV	MYO	LV	Avg.	Sup.	Sub.	TC	PE	ET	Avg.		
U-Net	0	3	36.6, 61.5	51.6, 20.7	57.9, 26.2	48.7, 36.2	0	10	57.5, 16.6	68.8, 22.9	74.7, 12.4	67.0, 17.3		
U-Net	0	140	90.6, 1.88	89.0, 3.59	94.6, 3.60	91.4, 3.02	0	876	75.8, 4.86	82.2, 5.87	83.6, 2.48	80.6, 4.40		
Mod	140	3	83.1, 11.1	80.7, 6.12	83.1, 14.7	82.3, 10.6	876	10	60.3, 7.69	76.2, 7.70	80.2, 4.97	72.3, 6.79		
NL [14]	140	3	61.0, 18.8	68.6, 13.7	81.5, 19.5	70.4, 17.3	876	10	59.5, 10.5	75.2, 8.35	76.8, 6.34	70.5, 8.40		
CPS [7]	140	3	80.2, 9.54	80.3, 3.17	86.3, 4.21	82.3, 5.64	876	10	62.9, 7.02	78.3, 7.08	80.8, 4.91	74.0, 6.24		
UAMT [26]	140	3	79.4, 7.81	77.7, 5.87	85.5, 8.16	80.9, 7.28	876	10	60.8, 9.84	78.4, 7.11	80.1, 4.24	73.3, 7.06		
Ours	140	3	87.2, 1.84	84.6, 2.70	90.1, 4.44	87.3, 2.99	876	10	65.5, 6.90	79.9, 6.38	80.8, 3.59	75.4, 5.62		

The quantitative results presented in Table 1 reveal that all methods that utilize additional superclass annotations outperformed the baseline method, which involved training a U-Net using only limited subclass labels. However, the methods that were specifically designed to utilize superclass information or explore the intrinsic structure of the subclass data, such as NL, CPS, and UAMT, did not consistently outperform the simple Modified U-Net. In fact, these methods sometimes performed worse than the simple Modified U-Net, indicating the difficulty of utilizing superclass information effectively. In contrast, our proposed method achieved the best performance among all compared methods on both the ACDC and BraTS2021 datasets. Specifically, our method attained an aver-

Table 2: Mean Dice Score (%), left) and HD_{95} (mm, right) of ablation studies on ACDC and BraTS2021 datasets (*mixup* and *pseudo* in HM column separately stands for using solely image mixup and pseudo-labeling to achieve better data utilization).

HM	PC	SN	ACDC								BraTS2021							
			Sup.	Sub.	RV	MYO	LV	Avg.	Sup.	Sub.	TC	PE	ET	Avg.				
			140	3	83.1, 11.1	80.7, 6.12	83.1, 14.7	82.3, 10.6	876	10	60.3, 7.69	76.2, 7.70	80.2, 4.97	72.3, 6.79				
	✓		140	3	85.9, 2.55	83.6, 3.70	89.8, 5.15	86.5, 3.80	876	10	65.0, 8.00	77.0, 7.47	80.6, 3.74	74.2, 6.40				
		✓	140	3	80.0, 8.06	80.4, 6.63	87.9, 5.07	82.8, 6.58	876	10	61.6, 7.00	77.3, 6.89	80.4, 6.01	73.1, 6.63				
		✓	140	3	79.0, 3.32	81.2, 3.69	88.6, 4.43	82.9, 3.82	876	10	63.5, 9.03	78.9, 6.29	80.2, 4.45	74.2, 6.59				
	✓	✓	140	3	85.1, 1.86	81.4, 4.29	87.3, 5.55	84.6, 3.90	876	10	65.1, 7.93	78.4, 6.86	78.3, 3.97	73.9, 6.25				
	✓	✓	140	3	87.6 , 2.81	83.8, 2.06	89.9, 2.87	87.1, 2.58	876	10	65.7, 7.56	79.6, 6.68	81.4 , 4.25	75.5, 6.16				
		✓	140	3	84.7, 5.26	84.1, 2.53	89.3, 2.79	86.0, 3.53	876	10	64.4, 7.96	79.5, 6.41	79.5, 5.07	74.4, 6.48				
<i>mixup</i>	✓	✓	140	3	82.9, 5.42	80.6, 4.18	86.8, 6.06	83.5, 5.22	876	10	66.2 , 6.90	79.6, 6.26	80.9, 4.19	75.6 , 5.79				
<i>pseudo</i>	✓	✓	140	3	78.8, 12.2	80.1, 7.66	84.3, 7.71	81.1, 9.20	876	10	62.4, 11.1	77.9, 6.55	80.0, 7.09	73.5, 8.24				
	✓	✓	140	3	87.2, 1.84	84.6 , 2.70	90.1 , 4.44	87.3 , 2.99	876	10	65.5, 6.90	79.9 , 6.38	80.8, 3.59	75.4, 5.62				
	✓	✓	140	6	86.6, 1.20	84.7, 1.87	90.9, 4.23	87.4, 2.44	876	20	70.7, 7.45	81.2, 6.08	82.2, 3.58	78.0, 5.70				
	✓	✓	140	9	86.1, 1.78	85.7, 1.92	90.8, 4.15	87.6, 2.62	876	30	71.4, 6.15	81.4, 5.84	82.5, 3.25	78.5, 5.08				
UNet			0	140	90.6, 1.88	89.0, 3.59	94.6, 3.60	91.4, 3.02	0	876	75.8, 4.86	82.2, 5.87	83.6, 2.48	80.6, 4.40				

age Dice score of 87.3% for ACDC and 75.4% for BraTS2021, outperforming the closest competitor by 5.0% and 1.4%, respectively.

Ablation studies In this study, we performed comprehensive ablation studies to analyze the contributions of each component and the performance of our method under different numbers of images with subclass annotations. The performance of each component is individually evaluated, and is listed in Table 2.

Each component has demonstrated its effectiveness in comparison to the naive modified U-Net method. Moreover, models that incorporate more components generally outperform those with fewer components. The effectiveness of the proposed HierarchicalMix is evident from the comparisons made with models that use only image mixup or pseudo-labeling for data augmentation, while the addition of Separate Normalization consistently improves the model performance. Furthermore, our method was competitive with a fully supervised baseline, achieving comparable results with only 6.5% and 3.4% subclass annotations on ACDC and BraTS2021.

4 Conclusion

In this work, we proposed an innovative approach to address the problem of efficient subclass segmentation in medical images, where limited subclass annotations and sufficient superclass annotations are available. To the best of our knowledge, this is the first work specifically focusing on this problem. Our approach leverages the hierarchical structure of categories to design network architectures and data generation methods that enable the network to distinguish between subclass categories more easily. Specifically, we introduced a Prior Concatenation module that enhances confidence in subclass segmentation by con-

catenating predicted logits from the superclass classifier, a Separate Normalization module that stretches the intra-class distance within the same superclass to facilitate subclass segmentation, and a HierarchicalMix model that generates high-quality pseudo labels for unlabeled samples by fusing only similar superclass regions from labeled and unlabeled images. Our experiments on the ACDC and BraTS2021 datasets demonstrated that our proposed approach outperformed other compared methods in improving the segmentation accuracy. Overall, our proposed method provides a promising solution for efficient fine-grained subclass segmentation in medical images.

References

1. Arazo, E., Ortego, D., Albert, P., O’Connor, N., McGuinness, K.: Pseudo-labeling and confirmation bias in deep semi-supervised learning. pp. 1–8 (07 2020)
2. Bai, W., Oktay, O., Sinclair, M., Suzuki, H., Rajchl, M., Tarroni, G., Glocker, B., King, A., Matthews, P.M., Rueckert, D.: Semi-supervised learning for network-based cardiac mr image segmentation. In: Medical Image Computing and Computer-Assisted Intervention- MICCAI 2017: 20th International Conference, Quebec City, QC, Canada, September 11-13, 2017, Proceedings, Part II 20. pp. 253–260. Springer (2017)
3. Baid, U., Ghodasara, S., Mohan, S., Bilello, M., Calabrese, E., Colak, E., Farahani, K., Kalpathy-Cramer, J., Kitamura, F.C., Pati, S., et al.: The rsna-asnr-miccai brats 2021 benchmark on brain tumor segmentation and radiogenomic classification. arXiv preprint arXiv:2107.02314 (2021)
4. Bakas, S., Reyes, M., Jakab, A., Bauer, S., Rempfler, M., Crimi, A., Shinohara, R.T., Berger, C., Ha, S.M., Rozycki, M., et al.: Identifying the best machine learning algorithms for brain tumor segmentation, progression assessment, and overall survival prediction in the brats challenge. arXiv preprint arXiv:1811.02629 (2018)
5. Bernard, O., Lalande, A., Zotti, C., Cervenansky, F., Yang, X., Heng, P.A., Cetin, I., Lekadir, K., Camara, O., Ballester, M.A.G., et al.: Deep learning techniques for automatic mri cardiac multi-structures segmentation and diagnosis: is the problem solved? *IEEE transactions on medical imaging* **37**(11), 2514–2525 (2018)
6. Bukchin, G., Schwartz, E., Saenko, K., Shahar, O., Feris, R., Giryas, R., Karlinsky, L.: Fine-grained angular contrastive learning with coarse labels. In: Proceedings of the IEEE/CVF Conference on Computer Vision and Pattern Recognition. pp. 8730–8740 (2021)
7. Chen, X., Yuan, Y., Zeng, G., Wang, J.: Semi-supervised semantic segmentation with cross pseudo supervision. In: Proceedings of the IEEE/CVF Conference on Computer Vision and Pattern Recognition. pp. 2613–2622 (2021)
8. Fotakis, D., Kalavasis, A., Kontonis, V., Tzamos, C.: Efficient algorithms for learning from coarse labels. In: Conference on Learning Theory. pp. 2060–2079. PMLR (2021)
9. Guo, S., Wang, L., Chen, Q., Wang, L., Zhang, J., Zhu, Y.: Multimodal mri image decision fusion-based network for glioma classification. *Frontiers in Oncology* **12** (2022)
10. Hansen, S., Gautam, S., Jenssen, R., Kampffmeyer, M.: Anomaly detection-inspired few-shot medical image segmentation through self-supervision with supervoxels. *Medical Image Analysis* **78**, 102385 (2022)

11. He, K., Zhao, W., Xie, X., Ji, W., Liu, M., Tang, Z., Shi, Y., Shi, F., Gao, Y., Liu, J., et al.: Synergistic learning of lung lobe segmentation and hierarchical multi-instance classification for automated severity assessment of covid-19 in ct images. *Pattern recognition* **113**, 107828 (2021)
12. Ioffe, S., Szegedy, C.: Batch normalization: Accelerating deep network training by reducing internal covariate shift. In: *International conference on machine learning*. pp. 448–456. pmlr (2015)
13. Kervadec, H., Dolz, J., Wang, S., Granger, E., Ayed, I.B.: Bounding boxes for weakly supervised segmentation: Global constraints get close to full supervision. In: *Medical imaging with deep learning*. pp. 365–381. PMLR (2020)
14. Kim, Y., Yim, J., Yun, J., Kim, J.: Nlnl: Negative learning for noisy labels. In: *Proceedings of the IEEE/CVF international conference on computer vision*. pp. 101–110 (2019)
15. Lei, W., Su, Q., Gu, R., Wang, N., Liu, X., Wang, G., Zhang, X., Zhang, S.: One-shot weakly-supervised segmentation in medical images. *arXiv preprint arXiv:2111.10773* (2021)
16. Luo, X.: SSL4MIS. <https://github.com/HiLab-git/SSL4MIS> (2020)
17. Luo, X., Wang, G., Liao, W., Chen, J., Song, T., Chen, Y., Zhang, S., Metaxas, D.N., Zhang, S.: Semi-supervised medical image segmentation via uncertainty rectified pyramid consistency. *Medical Image Analysis* **80**, 102517 (2022)
18. Ni, J., Cheng, W., Chen, Z., Asakura, T., Soma, T., Kato, S., Chen, H.: Superclass-conditional gaussian mixture model for learning fine-grained embeddings. In: *International Conference on Learning Representations* (2021)
19. Ouyang, C., Biffi, C., Chen, C., Kart, T., Qiu, H., Rueckert, D.: Self-supervision with superpixels: Training few-shot medical image segmentation without annotation. In: *Computer Vision—ECCV 2020: 16th European Conference, Glasgow, UK, August 23–28, 2020, Proceedings, Part XXIX* 16. pp. 762–780. Springer (2020)
20. Ronneberger, O., Fischer, P., Brox, T.: U-net: Convolutional networks for biomedical image segmentation. In: *Medical Image Computing and Computer-Assisted Intervention—MICCAI 2015: 18th International Conference, Munich, Germany, October 5–9, 2015, Proceedings, Part III* 18. pp. 234–241. Springer (2015)
21. Sekuboyina, A., Husseini, M.E., Bayat, A., Löffler, M., Liebl, H., Li, H., Tetteh, G., Kukačka, J., Payer, C., Štern, D., et al.: Verse: A vertebrae labelling and segmentation benchmark for multi-detector ct images. *Medical image analysis* **73**, 102166 (2021)
22. Tarvainen, A., Valpola, H.: Mean teachers are better role models: Weight-averaged consistency targets improve semi-supervised deep learning results. *Advances in neural information processing systems* **30** (2017)
23. Tu, P., Huang, Y., Zheng, F., He, Z., Cao, L., Shao, L.: Guidedmix-net: Semi-supervised semantic segmentation by using labeled images as reference. *Proceedings of the AAAI Conference on Artificial Intelligence* **36**, 2379–2387 (06 2022)
24. Wen, J., Varol, E., Sotiras, A., Yang, Z., Chand, G.B., Erus, G., Shou, H., Abdulkadir, A., Hwang, G., Dwyer, D.B., Pigoni, A., Dazzan, P., Kahn, R.S., Schnack, H.G., Zanetti, M.V., Meisenzahl, E., Busatto, G.F., Crespo-Facorro, B., Rafael, R.G., Pantelis, C., Wood, S.J., Zhuo, C., Shinohara, R.T., Fan, Y., Gur, R.C., Gur, R.E., Satterthwaite, T.D., Koutsouleris, N., Wolf, D.H., Davatzikos, C.: Multi-scale semi-supervised clustering of brain images: Deriving disease subtypes. *Medical Image Analysis* **75**, 102304 (2022)
25. Yang, J., Yang, H., Chen, L.: Towards cross-granularity few-shot learning: coarse-to-fine pseudo-labeling with visual-semantic meta-embedding. In: *Proceedings of the 29th ACM International Conference on Multimedia*. pp. 3005–3014 (2021)

26. Yu, L., Wang, S., Li, X., Fu, C.W., Heng, P.A.: Uncertainty-aware self-ensembling model for semi-supervised 3d left atrium segmentation. In: Medical Image Computing and Computer Assisted Intervention–MICCAI 2019: 22nd International Conference, Shenzhen, China, October 13–17, 2019, Proceedings, Part II 22. pp. 605–613. Springer (2019)
27. Zhang, K., Zhuang, X.: Cyclemix: A holistic strategy for medical image segmentation from scribble supervision. In: Proceedings of the IEEE/CVF Conference on Computer Vision and Pattern Recognition. pp. 11656–11665 (2022)

5 Supplementary Materials

Table 3: Training parameters on ACDC and BraTS2021 datasets.

Parameter	ACDC	BraTS2021
GPU	One Nvidia 3090 GPU	
Program language	Python 3.7.13	
Training framework	PyTorch 1.10.0	
Base learning rate	0.01	
Total iterations	40000	
Batch size	24	4
Patch size	256×256	$96 \times 96 \times 96$
Memory Usage	8GB	10GB

Table 4: Training time (days) of different methods on ACDC and BraTS2021 datasets.

Dataset	U-Net	Mod	NL	CPS	UAMT	Ours
ACDC	0.12	0.22	0.14	0.31	0.21	0.23
BraTS2021	0.78	1.77	0.80	3.83	2.60	2.56

Table 5: Mean Dice Score (% , left) and HD_{95} (mm, right) and their standard deviations of different methods on ACDC dataset. Sup. and Sub. separately represents the number of data with superclass and subclass annotations in the experiments. ‘_’ means the result of our proposal is significantly better than the closet competitive result (p-value < 0.05).

Method	Sup.	Sub.	LV	MYO	RV	Avg.
U-Net	0	3	36.6±29.1, 61.5±30.0	51.6±30.0, 20.7±23.6	57.9±34.3, 26.2±32.0	48.7±30.0, 36.2±2.2
U-Net	0	140	90.6±6.32, 1.88±4.12	89.0±2.96, 3.59±10.6	94.6±3.59, 3.60±10.1	91.4±2.92, 3.02±5.77
Mod	140	3	83.1±9.33, 11.1±24.6	80.7±6.43, 6.12±6.98	83.1±13.3, 14.7±13.7	82.3±8.00, 10.6±10.2
NL	140	3	61.0±26.0, 18.8±16.3	68.6±20.6, 13.7±14.4	81.5±14.1, 19.5±19.8	70.4±18.3, 17.3±12.7
CPS	140	3	80.2±9.99, 9.54±12.9	80.3±7.40, 3.17±4.47	86.3±10.4, 4.21±10.3	82.3±7.28, 5.64±5.68
UAMT	140	3	79.4±11.7, 7.81±13.7	77.7±9.73, 5.87±8.74	85.5±11.2, 8.16±10.5	80.9±9.21, 7.28±8.56
Ours	140	3	87.2±7.44 , 1.84±1.84	84.6±4.97 , 2.70±4.87	90.1±9.25 , 4.44±10.4	87.3±5.33 , 2.99±4.40

Table 6: Mean Dice Score (% , left) and HD_{95} (mm, right) and their standard deviations of different methods on BraTS2021 dataset. Sup. and Sub. separately represents the number of data with superclass and subclass annotations in the experiments. ‘_’ means the result of our proposal is significantly better than the closet competitive result (p-value < 0.05).

Method	Sup.	Sub.	TC	PE	ET	Avg.
U-Net	0	10	57.5±29.1, 16.6±22.5	68.8±22.1, 22.9±26.2	74.7±21.6, 12.4±21.8	67.0±20.0, 17.3±19.2
U-Net	0	876	75.8±23.9, 4.86±9.26	82.2±15.8, 5.87±9.72	83.6±17.4, 2.48±4.16	80.6±14.9, 4.40±5.84
Mod	876	10	60.3±28.5, 7.69±7.73	76.2±18.3, 7.70±9.01	80.2±17.6, 4.97±8.47	72.3±17.7, 6.79±6.11
NL	876	10	59.5±28.4, 10.5±15.1	75.2±15.8, 8.35±11.4	76.8±20.5, 6.34±12.6	70.5±16.2, 8.40±9.98
CPS	876	10	62.9±26.8, 7.02±7.97	78.3±18.4, 7.08±10.1	80.8±17.8, 4.91±9.79	74.0±17.0, 6.24±7.90
UAMT	876	10	60.8±26.7, 9.84±10.7	78.4±17.4, 7.11±9.97	80.1±18.0, 4.24±6.40	73.3±16.3, 7.06±6.18
Ours	876	10	65.5±26.6, 6.90±9.63	79.9±17.3, 6.38±9.32	80.8±18.6, 3.59±8.34	75.4±16.5, 5.62±6.45